processes

MDPI

Article

High-Efficiency Desulfurization of High-Sulfur Bauxite Calcined in a Conveyor Bed: Kinetics, Process, and Application

Shaowu Jiu, Bo Zhao and Yanxin Chen *

College of Materials and Engineering, Xi'an University of Architecture and Technology, Xi'an 710055, China
* Correspondence: chen_yanxin@xauat.edu.cn

Abstract: The reaction process, mechanism, and kinetics of the desulfurization of high-sulfur bauxite during calcination were investigated using thermal analysis–infrared analysis. A conveyor-bed calcination system was used to study the variations in the physical phase, desulfurization rate, and alumina dissipation rate of high-sulfur bauxite in the range of 500 °C–650 °C. The results show that sclerite monohydrate, kaolinite, rhodochrosite, pyrite, and dolomite mainly decompose during the calcination of high-sulfur bauxite, generating $H_2O_{(g)}$, CO_2, and SO_2 as gaseous products. The decomposition of sclerite monohydrate and kaolinite and the dehydroxylation reactions of rhodochrosite and pyrite occur at <650 °C, with inseparable temperature overlap. High-sulfur bauxite desulfurization follows a three-dimensional spherical diffusion mechanism, with an activation energy of 181.16 kJ/mol, controlled by the diffusion rate of O_2 or SO_2 through the solid product layer. High-sulfur bauxite was calcined at 600 °C–650 °C for around 3.5 s in a conveyor bed, resulting in a negative divalent sulfur content of <0.03 wt.%, desulfurization rate of >0.98, and relative dissolution rate of alumina of >99%, satisfying the requirements of aluminum extraction via the Bayer method. The desulfurization rate predictions of the kinetic model were consistent with the experimental data.

Keywords: high-sulfur bauxite; desulfurization in conveyor bed; kinetics; reaction mechanism; alumina digestion

check for updates

Citation: Jiu, S.; Zhao, B.; Chen, Y. High-Efficiency Desulfurization of High-Sulfur Bauxite Calcined in a Conveyor Bed: Kinetics, Process, and Application. *Processes* **2022**, *10*, 1586. https://doi.org/10.3390/pr10081586

Academic Editor: Luis Puigjaner

Received: 17 July 2022
Accepted: 10 August 2022
Published: 12 August 2022

Publisher's Note: MDPI stays neutral with regard to jurisdictional claims in published maps and institutional affiliations.

Copyright: © 2022 by the authors. Licensee MDPI, Basel, Switzerland. This article is an open access article distributed under the terms and conditions of the Creative Commons Attribution (CC BY) license (https://creativecommons.org/licenses/by/4.0/).

1. Introduction

Bauxite is the raw material used in the industrial production of aluminum in its metallic form. Bauxite with a sulfur content of >0.7% by mass is referred to as high-sulfur bauxite [1]. The bauxite reserves in China total 4.2 billion tons, 560 million tons of which is high-sulfur bauxite [2]. In high-sulfur bauxite, >90% of the sulfur exists in the form of iron (II) disulfide (FeS_2) [3]. During the production of alumina via the Bayer process, the sulfide (S_2^{2-}) in high-sulfur bauxite is gradually transformed into thiosulfate ($S_2O_3^{2-}$), sulfite (SO_3^{2-}), and sulfate (SO_4^{2-}), which can lead to a series of problems, such as equipment corrosion, lye consumption, reduction in product purity, and an influence on red mud settling [4–8]. These problems are the reasons why high-sulfur bauxite ores cannot be directly utilized. With the increasing scarcity of high-quality mineral resources, it is thus of practical significance to investigate the desulfurization of high-sulfur bauxite ores.

The key method for the utilization of high-sulfur bauxite is the removal of negative divalent sulfur, thereby resulting in a total sulfur content of <0.4% to meet the requirements of the Bayer method [3]. High-sulfur bauxite can be desulfurized via flotation, roasting, and digestion [9–12]. Roasting desulfurization has the advantages of a high desulfurization rate and the ore exhibiting a loose structure after roasting, which is conducive to aluminum leaching and is therefore considered to be an ideal desulfurization technology. There are three main processes for the roasting and desulfurization of high-sulfur bauxite: rotary-kiln, fluidized-bed, and conveyor-bed methods [13,14]. In rotary-kiln and fluidized-bed processes, high-sulfur bauxite needs to be calcined at a minimum temperature of 750 °C for at least 10 min [15–18]. However, in the conveyor-bed process, high-sulfur bauxite can

be completely desulfurized only upon calcination for 3–5 s in the temperature range of 600 °C–700 °C [3]. Compared to the rotary-kiln and fluidized-bed calcination processes, the use of conveyor-bed technology has obvious advantages in terms of energy saving and high efficiency. Due to the short calcination time of the conveyor-bed process, the desulfurization of high-sulfur bauxite is very sensitive to the effect of temperature and time parameters. Therefore, it is necessary to establish an accurate desulfurization kinetic model to provide a basis for process design and production control.

At present, reaction kinetics is mainly based on thermal analysis technology [19,20]. The reaction conversion rate data are calculated from the mass change of the sample or heat data during the reaction process, and the reaction kinetic parameters are then calculated [21]. Due to the complex composition of high-sulfur bauxite and its extremely low content of sulfur minerals (usually <3%), the mass and heat changes that arise due to the desulfurization reaction during calcination are difficult to elucidate. Therefore, it is very difficult to characterize the desulfurization kinetics of high-sulfur bauxite. The gaseous product sulfur dioxide (SO_2) formed via the desulfurization reaction of high-sulfur bauxite exhibits significant infrared (IR) absorption characteristics, which can be detected by combined thermal analysis–IR analysis technology [22]. Therefore, by detecting and quantifying the SO_2 content in the gas evolved from the reaction, the characteristics of the desulfurization reaction can be extracted. The authors developed a method to calculate complex reaction kinetics based on the release characteristics of gaseous products using a combined thermal analysis–IR analysis technique [23]. Satisfactory results were obtained for the calcination reaction mechanism and kinetic analysis of coal gangue using this method, providing a basis for the desulfurization mechanism and kinetic analysis of high-sulfur bauxite. However, at present, there is still a lack of systematic work on the mechanism and kinetics of high-sulfur bauxite desulfurization. Therefore, it is necessary to carry out in-depth research for the development of conveyor-bed desulfurization technology.

In this study, high-sulfur bauxite was used as a raw material. Thermal analysis–IR analysis was used to characterize the gas product composition, release curves, reaction mechanism, and desulfurization reaction kinetics. The desulfurization reaction of high-sulfur bauxite at different temperatures was predicted using kinetic equations, and experiments were conducted on a conveyor-bed calcining system. X-ray diffraction analysis (XRD), sulfur content analysis, scanning electron microscopy (SEM), and energy-dispersive X-ray spectroscopy analysis (EDS) were performed on desulfurized bauxite samples to evaluate the effectiveness of the conveyor-bed desulfurization process. The results of this study thus serve as a reference for the development, process design, and production control of high-sulfur bauxite conveyor-bed desulfurization technology.

2. Materials and Methods

2.1. Raw Materials

High-sulfur bauxite was procured from Nanchuan, Chongqing, China. The proven reserves of high-sulfur bauxite in Nanchuan are about 100 million tons, which mainly occurs in the sedimentary environment of the paleo-residual facies of the Middle Permian system. The deposit type belongs to the weathering–sedimentation–transformation deposit of the in situ sedimentary type of the ancient weathering crust, with the weathered residual clay rock and bauxite as the parent. A total of 50 t of high-sulfur bauxite was collected in the experiment, and 20 kg of high-sulfur bauxite was collected by the method of multi-point sampling for analysis. High-sulfur bauxite was dried in an oven at 105 °C ± 0.5 °C before being ground into a fine powder with a particle size of <80 μm (d_{50} = 47.28 μm). The resulting powdered high-sulfur bauxite was then analyzed by X-ray diffractometry (XRD, D/MAX-2200 X-ray diffractometer, Rigaku) using a CuKα X-ray source, operating at a tube voltage of 45 kV and a tube current of 40 mA, with measurements conducted over a 2θ range of 5° to 75°. The chemical composition of high-sulfur bauxite was analyzed by X-ray fluorescence spectroscopy (XRF, S4PIONEER, Bruker, Germany) operated at X-ray tube parameters of 4.2 kW, 60 kV (max), and 140 mA (max). The barium sulfate gravimetric

method was adopted for the analysis of sulfur minerals. The XRD pattern of high-sulfur bauxite is shown in Figure 1. The average results of XRF spectroscopy analysis with 10 samples are shown in Table 1.

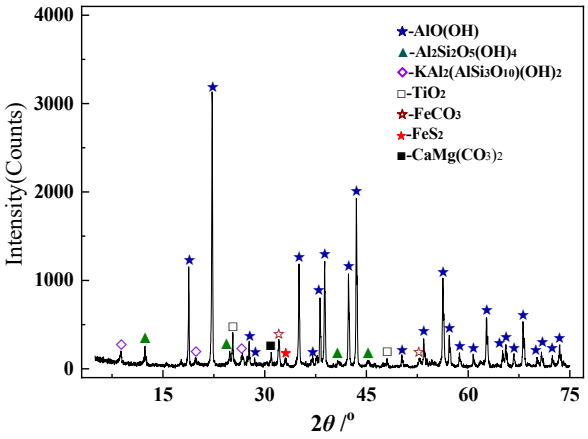


Figure 1. XRD pattern of high-sulfur bauxite.

Table 1. Chemical composition of high-sulfur bauxite in wt.%.

Al_2O_3	SiO_2	Fe_2O_3	CaO	MgO	TiO_2	S_{Total}	S_2^{2-}
65.78	8.16	5.48	0.56	0.37	3.15	1.42	1.29

The aluminum-containing minerals in the raw material are mainly in the form of diaspore, kaolinite, and muscovite, of which diaspore is the main component. Sulfur mainly exists in the form of pyrite, in addition to impurities such as siderite and dolomite. The total sulfur content is 1.42 wt.%, of which the negative divalent sulfur content is 1.29 wt.%.

2.2. Combined Thermal Analysis–IR Analysis Experiment

The mass, heat, and gas products during the calcination of high-sulfur bauxite were detected using a combined thermal analysis–infrared analysis system. Thermal analysis was performed on a synchronous thermal analyzer (NETZSCH 409PC TGA-DSC, Germany), and IR analysis was performed on an IR spectrometer (Bruker FTIR-7600) in air at a flow rate of 70.0 mL/min using a sample mass of 10.0 ± 0.5 mg at heating rates of 5 °C/min, 10 °C/min, 15 °C/min, or 20 °C/min. Fourier-transform IR (FTIR) spectroscopy was used to detect the composition of the gaseous products over a wavenumber range of 4000 cm^{-1}–600 cm^{-1}. The SO_2 release curve was extracted from the FTIR spectrum to analyze the characteristics of the high-sulfur bauxite desulfurization reaction.

2.3. Kinetic Analysis Method

The kinetic equation for the reaction of solid matter is as follows: [19,24]

$$d\alpha/dt = A \cdot \exp[-E/(RT)] \cdot f(\alpha) \quad (1)$$

In Equation (1): α is the reaction conversion rate; t is the time in s; A is the pre-exponential factor of the kinetic equation in s^{-1}; E is the reaction activation energy in kJ/mol; R is the gas constant, the value of which is 8.314 J/(mol·K); T is the temperature in K; and $f(\alpha)$ is the differential form of the mechanism function.

In the thermal analysis measurements, the heating rate β is constant, so the relationship between temperature T and time t is:

$$T = T_0 + \beta t \quad (2)$$

where T_0 is the initial temperature, K. Differentiating both sides of Equation (2) simultaneously gives:

$$dT = \beta dt \text{ (or } dt = dT/\beta) \quad (3)$$

Equation (3) can be substituted into Equation (1) to give:

$$d\alpha/dT = (A/\beta)\cdot\exp[-E/(RT)]\cdot f(\alpha) \quad (4)$$

Equation (4) is a thermal analysis kinetic equation in differential form and can be integrated to obtain a kinetic equation in integral form:

$$G(\alpha) = A\cdot\exp(-E/RT)\cdot t \quad (5)$$

where $G(\alpha)$ is the integral form of the mechanism function, and the commonly used $G(\alpha)$ functions for solid-phase reactions are shown in Table 2.

Table 2. Common mechanism functions of $G(\alpha)$ for solid-state reactions [23,25].

Symbol of $G(\alpha)$	Sequence Number of Function	Equation Name	Expression of $G(\alpha)$ Function
D1	1	One-dimensional diffusion	α^2
D2	2	Two-dimensional diffusion	$\alpha + (1-\alpha)\ln(1-\alpha)$
1D3	6	Tridimensional diffusion (spherically symmetric)	$[1-(1-\alpha)^{1/3}]^2$
A3	11	Nucleation and growth ($n = 1/3$)	$[-\ln(1-\alpha)]^{1/3}$
A2	13	Nucleation and growth ($n = 1/2$)	$[-\ln(1-\alpha)]^{1/2}$
A1	16	Nucleation and growth ($n = 1$)	$-\ln(1-\alpha)$
P3	23	Power law	$\alpha^{1/3}$
P2	24	Power law	$\alpha^{1/2}$
R3	29	Shrinking core (spherically symmetric)	$1-(1-\alpha)^{1/3}$
R2	31	Shrinking core (cylindrically symmetric)	$1-(1-\alpha)^{1/2}$
C2	37	Chemical reaction	$(1-\alpha)^{-1}-1$

The purpose of kinetic analysis is to solve E, A, and $G(\alpha)$ using kinetic Equation (4) or Equation (5). Solving the kinetic equations requires calculating the reaction conversion α from experimental data. In this study, the conversion rate of the desulfurization reaction was calculated from the SO_2 gas release data, rather than the traditional thermogravimetric (TG) or differential scanning calorimetry (DSC) data. The following equation was used to calculate the reaction conversion rate α:

$$\alpha = S_T/S_{total} \quad (6)$$

where S_T is the integral area of the SO_2 release curve, and S_{total} is the total integral area of the SO_2 release curve.

The $\alpha - T$ data were fitted using both the Kissinger and general integration methods to obtain kinetic parameters, where the Kissinger method equation is [26]:

$$\ln\left(\frac{\beta_i}{{T_{pi}}^2}\right) = \ln\frac{AR}{E} - \frac{E}{R}\frac{1}{T_{pi}},\ i = 1,\ 2,\ 3,\ 4 \quad (7)$$

where β_i is the heating rate in °C/min, and T_{pi} is the peak temperature of the derivative thermogravimetry (DTG) curve in K.

The general equation for calculating the integrals is [27]:

$$\ln\left[\frac{G(\alpha)}{T^2}\right] = \ln\left\{\frac{AR}{\beta E}\left(1 - \frac{2RT}{E}\right)\right\} - \frac{E}{RT} \quad (8)$$

For a suitable $G(\alpha)$, $\ln[G(\alpha)/T^2] - 1/T$ in Equation (8) shows a linear relationship, so the E value is obtained from the slope of the straight line, and the A value is obtained from the intercept. E, A, and $G(\alpha)$ can be incorporated into Equation (2) to obtain the kinetic equation for the desulfurization of high-sulfur bauxite. The effect of temperature and time on the reaction conversion rate α can then be predicted from the kinetic equation.

2.4. Conveyor-Bed Desulfurization Experiments

The experimental set-up for conveyor-bed calcination is shown in Figure 2. The system consists of a hot blast stove, feeder, suspension reactor, separator, dust collector, product bin, centrifugal fan, and SO_2 absorption device, with air used in combustion and kerosene as a hot blast stove fuel. The feeder consists of a silo and a screw conveyor. The suspension reactor is a tubular structure made of heat-resistant stainless steel, and the outer part of the furnace body is covered with a compensation-type electric heating sleeve. The separator is a cyclone with a separation efficiency of around 90%. The dust collector is a bag-type structure that captures the fines escaping from the cyclone. The powder collected by the cyclone and bag filter enters the product bin, which is a closed cylinder. The system is operated under negative pressure and powered by a centrifugal fan. The absorbent in the SO_2 absorption device is low-concentration lye, and the exhaust gas is discharged after purification.

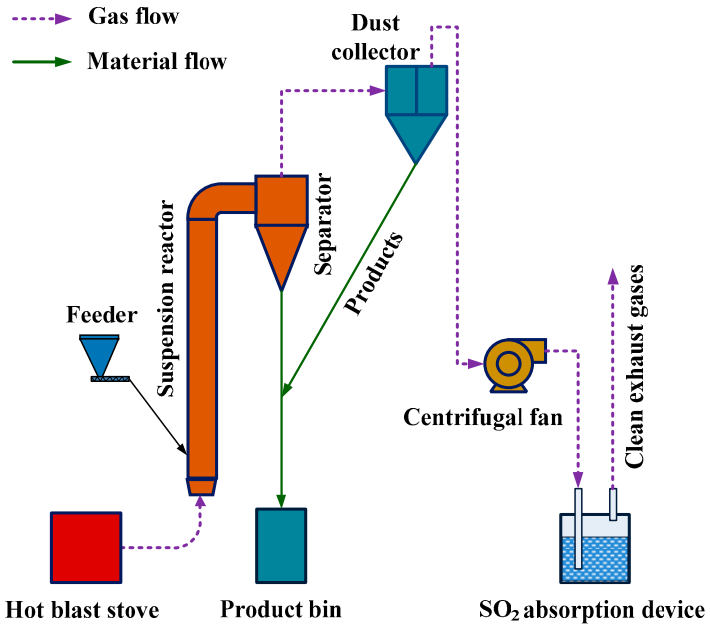


Figure 2. Overview of the system used in the conveyor-bed calcination process.

During experiments, the calcination temperature (the temperature in the middle of the furnace body) was controlled in the range of 600 °C–750 °C, the residence time was around 3.5 s, and the feed rate per hour was 20 ± 0.5 kg.

2.5. Product Characterization

The main elements in bauxite were detected by XRF spectroscopy. The phase composition and crystallite structure of the product were analyzed by XRD. The morphology characteristics of high-sulfur bauxite before and after calcination were analyzed by SEM. The mass fractions of total sulfur and sulfate sulfur were analyzed using the barium sulfate gravimetric

method, and the sulfur content in sulfide was then calculated by subtracting the two, with the desulfurization rate calculated according to a literature method [3]. Alumina digestion analysis of roasted high-sulfur bauxite ore was conducted via digestion at 250 °C for 60 min.

3. Results and Discussion

3.1. Combined Thermal Analysis–IR Analysis Experiments

The TG and DTG data of the thermal analysis of high-sulfur bauxite are shown in Figures 3a and 3b, respectively.

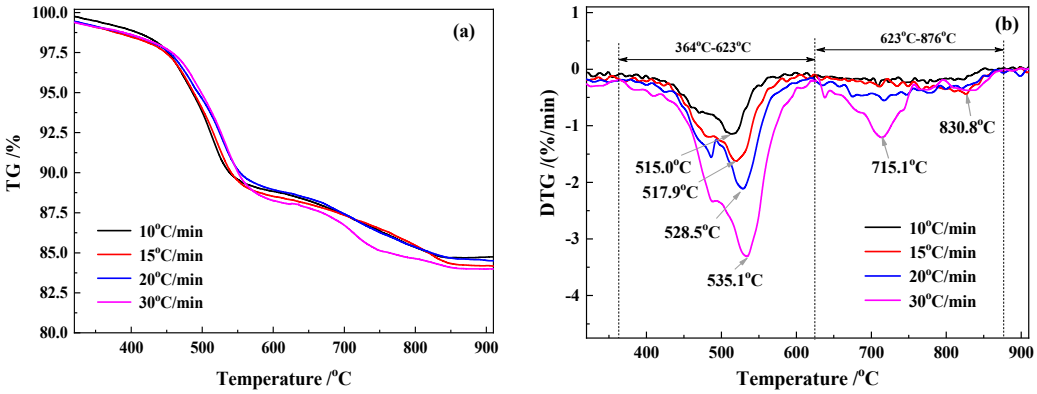


Figure 3. (**a**) TG and (**b**) DTG data of high-sulfur bauxite.

As shown in Figure 3a,b, the mass loss of high-sulfur bauxite in the calcination process mainly proceeded via two stages. The first stage, which was the main stage of the reaction, was in the range of 364 °C–623 °C, representing a rate of change in mass of −10.96% to −10.71%. Figure 3b shows an overlapping of peaks in the DTG curve, indicating that this stage does not involve a single reaction. The second stage is observed over a temperature range of 623 °C–876 °C, representing a rate of change in mass from −3.91% to −3.73%. Two peaks are present in the DTG curve recorded at 30 °C/min but are not observed at other heating rates, indicating that two-step reactions also occurred that could not be clearly distinguished at this stage.

The reaction process of high-sulfur bauxite was further analyzed via the IR spectroscopic analysis of the gaseous products. The three-dimensional IR absorption spectrum of the evolved gas recorded at a heating rate of 10 °C/min is shown in Figure 4a, and the two-dimensional IR absorption spectrum obtained from Figure 4a is shown in Figure 4b.

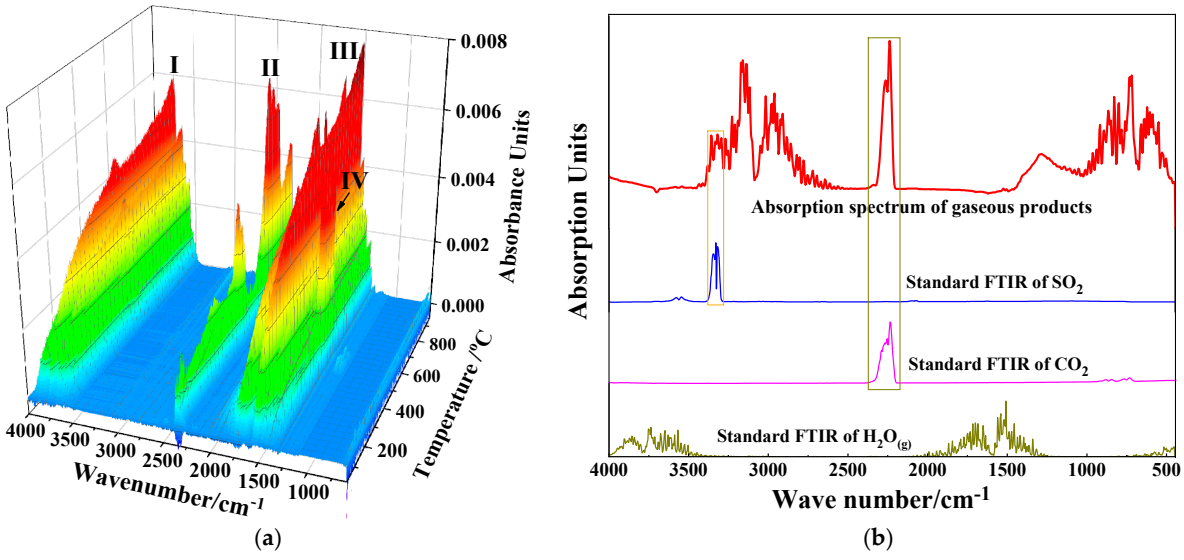


Figure 4. (**a**) Three-dimensional and (**b**) two-dimensional FTIR spectra of the gaseous products.

As shown in Figure 4b, the gaseous products released from the decomposition of high-sulfur bauxite mainly feature three functional groups: hydroxyl, carbonyl, and S–O groups. The gaseous product components corresponding to hydroxyl, carbonyl, and S–O groups are $H_2O_{(g)}$, CO_2, and SO_2, respectively, determined with reference to the standard spectral library. Inferred from the chemical composition of high-sulfur bauxite, $H_2O_{(g)}$ is produced via the decomposition of diaspore, kaolinite, and muscovite, among which the decomposition of diaspore is dominant, CO_2 is produced via the decomposition of siderite and calcite, and SO_2 is produced by the decomposition of pyrite. The relevant reaction equations relating to these decomposition reactions are as follows:

$$2AlO(OH) \rightarrow Al_2O_3 + H_2O_{(g)}\uparrow \quad (9)$$

$$Al_2O_3 \cdot 2SiO_2 \cdot 2H_2O \rightarrow Al_2O_3 \cdot 2SiO_2 + 2H_2O_{(g)}\uparrow \quad (10)$$

$$4FeCO_3 + O_2 \rightarrow 2Fe_2O_3 + 4CO_2\uparrow \quad (11)$$

$$CaMg(CO_3)_2 \rightarrow MgO + CaO + 2CO_2\uparrow \quad (12)$$

$$2FeS_2 + 5.5O_2 \rightarrow Fe_2O_3 + 4SO_2(g)\uparrow \quad (13)$$

$$KAl_2(Si_3Al)O_{10}(OH)_2 \rightarrow KAl_2(Si_3Al)O_{11} + H_2O_{(g)}\uparrow \quad (14)$$

According to the analysis results of Figure 4b, the peaks labeled I and III in Figure 4a are the IR absorption peaks of $H_2O_{(g)}$, the peak labeled II is the IR absorption peak of CO_2, and the peak labeled IV is the IR absorption peak of SO_2. The intensity of the IR absorption peaks is related to the amount of gaseous products released. The release flow curves of $H_2O_{(g)}$, CO_2, and SO_2 were determined from Figure 4a and are shown in Figure 5.

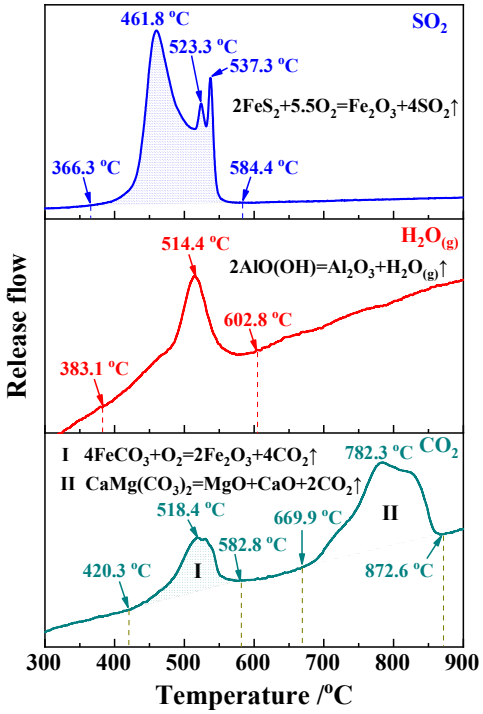


Figure 5. Release flow curves of the gaseous products SO_2, $H_2O_{(g)}$, and CO_2.

As shown in Figure 5, the release of SO_2 is observed in the range of 366.3 °C–584.4 °C, with three overlapping peaks with peak temperatures of 461.8 °C, 523.3 °C, and 537.3 °C observed in the flow curve, which indicates that the desulfurization reaction of high-sulfur alumina is also a multistep reaction. There is only one peak in the release curve of $H_2O_{(g)}$, indicating that the dehydroxylation reaction of high-sulfur bauxite is a continuous process. The left slope of the $H_2O_{(g)}$ release peak is small but suddenly increases at 482 °C. The

release flow was the greatest at 514.4 °C, and then the release flow continued to decrease up to 602.8 °C. The release process of CO_2 involves two steps. The first reaction occurs between 420.3 °C and 582.8 °C, with the second reaction occurring in the temperature range of 669.9 °C–872.6 °C. The decomposition temperature of siderite is usually <600 °C, while that of dolomite is usually >650 °C. Therefore, it can be determined that the first-step decarburization reaction corresponds to the decomposition of siderite, with the second-step reaction corresponding to the decomposition of dolomite. Dolomite is actually a eutectic mineral of calcium carbonate and magnesium carbonate. The decomposition temperature of magnesium carbonate is lower than that of calcium carbonate, so the decomposition of dolomite is also a two-step reaction, consistent with the presence of two overlapping peaks in the second-step release CO_2 curve shown in Figure 5. According to Figures 3 and 5, the reaction of high-sulfur bauxite in the temperature range of 380 °C–605 °C can be attributed to the decomposition of pyrite, diaspore, kaolinite, and siderite. The temperature ranges of these reactions overlap, with the decomposition of diaspore accompanied by the calcination and desulfurization of high-sulfur bauxite. In the temperature range of 670 °C–900 °C, the decomposition of dolomite mainly occurs. The desulfurization reaction of high-sulfur bauxite occurs in the temperature range of 366.3 °C–584.7 °C, with full desulfurization achieved at a calcination temperature of >600 °C.

3.2. Kinetic Analysis

For the comprehensive utilization of high-sulfur bauxite, desulfurization is the key reaction [14,16,17]. The kinetics of the desulfurization reaction is an important basis for determining the parameters of the calcination temperature and time. The negative divalent sulfur content in high-sulfur bauxite is only 1.29 wt.%, with its desulfurization overlapping with the dehydroxylation reaction, so the TG data cannot be used to perform kinetic analysis. In this study, the SO_2 release flow curves were used to calculate the kinetics of the desulfurization reaction. The FTIR data collected at 10 °C/min, 15 °C/min, 20 °C/min, and 30 °C/min were integrated according to Equation (6) to obtain a curve for the conversion rate α, which is shown in Figure 6. The Kissinger method was used for kinetic calculations using the DTG peak temperature data. The general integration method was applied to the data shown in Figure 7 $\alpha - T$, selecting the mechanism functions in Table 2 in turn for fitting. The results show that mechanism function No. 6 has the highest linearity. The fittings of the general integration method and the Kissinger method are shown in Figure 7a and Figure 7b, respectively, with the fitting results of Figure 7 listed in Table 3.

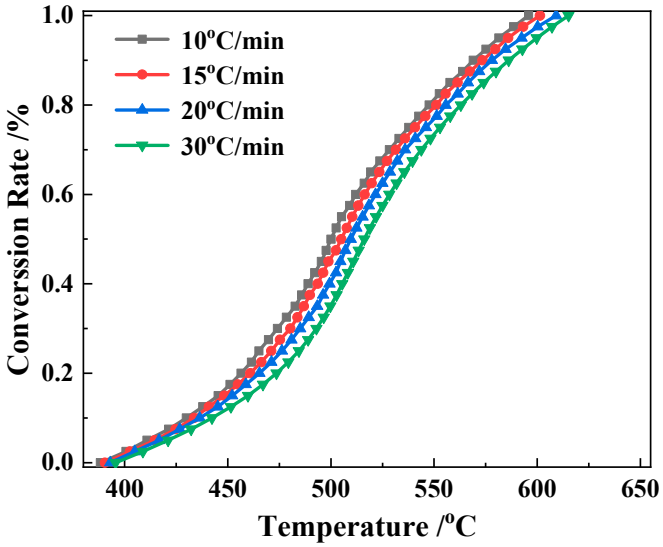


Figure 6. Conversion rate curves.

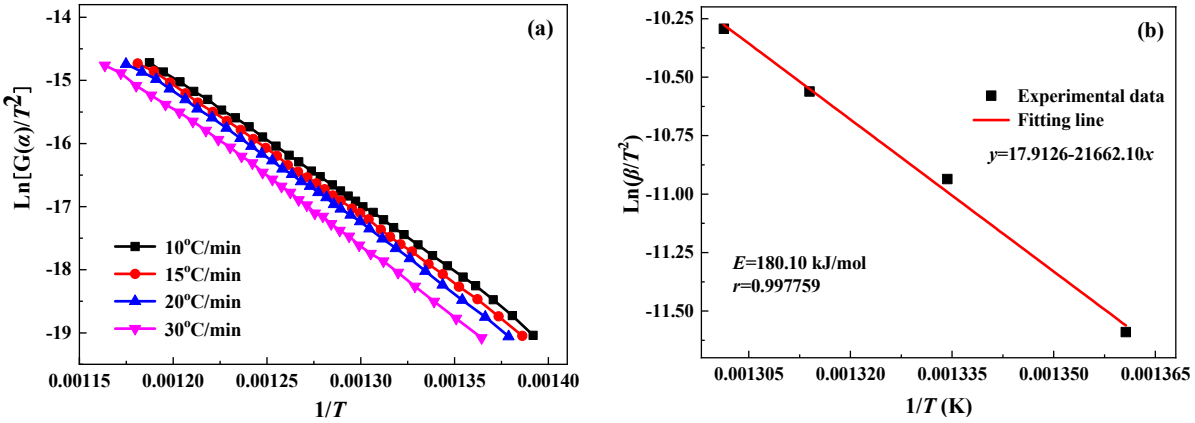


Figure 7. Kinetic fitting curves of the (**a**) general integral and (**b**) Kissinger methods.

Table 3. Reaction kinetics fitting results.

Method	*B*/(°C/min)	*E*/(kJ/mol)	*A*	*r*
General integral method	10	175.87	9.53×10^8	0.990204
	15	180.22	1.63×10^9	0.990701
	20	182.29	1.87×10^9	0.991385
	30	186.26	2.65×10^9	0.989086
	Average value	181.16	1.77×10^9	0.990344
Kissinger method	——	180.10	——	0.997759

As shown in Table 3, the linear correlation coefficients of the fitting of mechanism function No. 6 using the general integration and Kissinger methods were >0.989. At the same time, the activation energies obtained using the two methods are very close (the relative deviation is only 0.59%), indicating that the kinetic fitting results in Table 4 are reasonable. Mechanism function No. 6 represents three-dimensional diffusion (spheres), indicating that the desulfurization reaction of high-sulfur bauxite is controlled by the rate of the diffusion of O_2 or SO_2 via the solid product layer. Taking the average value of the general integration method as the final result, the kinetic equation of the calcination reaction of coal series kaolinite was obtained as follows:

$$\left[1-(1-\alpha)^{\frac{1}{3}}\right]^2 = 1.77 \times 10^9 exp\left(-\frac{181.16}{RT}\right) \cdot t \quad (15)$$

Table 4. Analysis results of the desulfurization rate of roasted high-sulfur bauxite.

Temperature (°C)	Al_2O_3 (wt.%)	St (wt.%)	Sulfate Sulfur (wt.%)	Sulfide Sulfur (wt.%)	Desulfurization Rate	
					Experimental Data	Predicted Data
Raw ore	66.90	1.42	0.13	1.29	0.00	0.00
500	68.3	0.83	0.17	0.66	0.50	0.47
525	67.5	0.68	0.19	0.49	0.62	0.65
550	70.05	0.5	0.23	0.27	0.80	0.83
575	70.67	0.41	0.32	0.09	0.93	0.96
600	71.95	0.38	0.35	0.03	0.98	1.00
625	72.47	0.36	0.35	0.01	0.99	1.00
650	74.83	0.35	0.35	0.00	1.00	1.00

Note: The desulfurization rates were calculated using a literature method.

The kinetic equation characterizes the effects of calcination temperature T and time t on the desulfurization reaction process (conversion α). The desulfurization reaction conversion of high-sulfur bauxite in the range of 500 °C–650 °C was predicted by the kinetic equation, with the results shown in Figure 8.

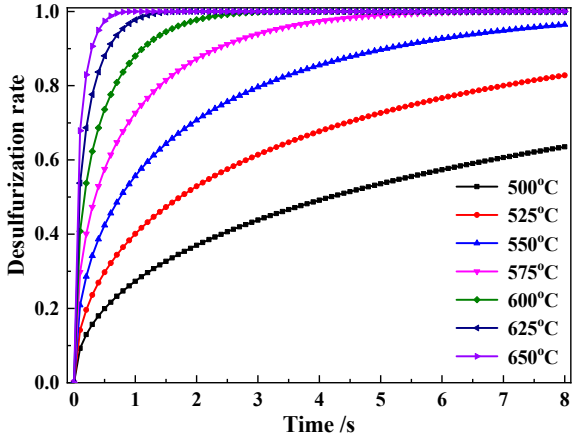


Figure 8. Desulfurization reaction curves predicted using the kinetic equation.

The kinetic prediction results show that the time required for complete desulfurization of high-sulfur bauxite was 8.0 s, 3.9 s, 2.0 s, and 1.0 s, respectively, upon its calcination at 575 °C, 600 °C, 625 °C, and 650 °C. The complete desulfurization of high-sulfur bauxite in the temperature range of 575 °C–650 °C required only a few seconds, showing that it provides a theoretical basis for transport-bed suspension calcination technology.

3.3. Characterization of Calcined Products in a Conveyor Bed

3.3.1. Desulfurization Rate Analysis

High-sulfur bauxite was calcined at different temperatures from 500 °C to 650 °C at a residence time of around 3.5 s using the conveyor-bed calcination desulfurization experimental system. The analysis results of Al_2O_3, total sulfur, sulfur in sulfate, and negative divalent sulfur in roasted ore samples are shown in Table 4.

According to the data in Table 4, the influence of calcination temperature on the sulfur content and desulfurization rate in high-sulfur bauxite was determined, with the results shown in Figure 9.

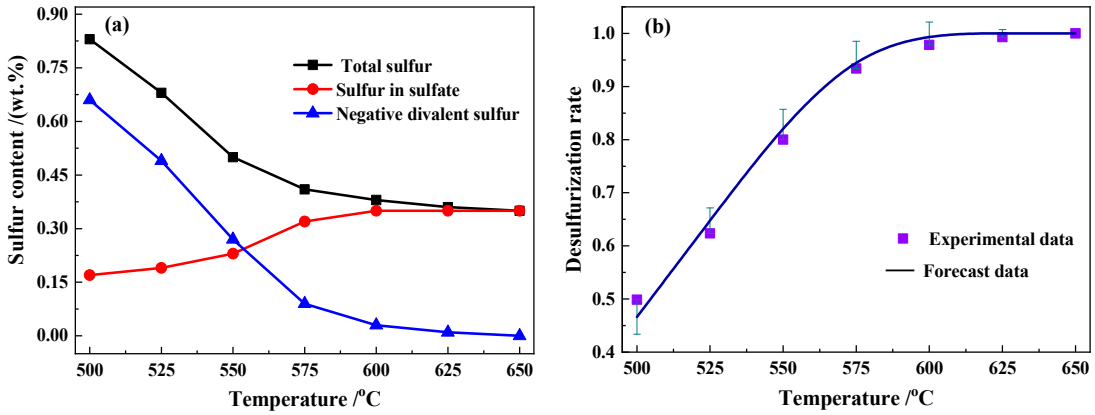


Figure 9. Effect of temperature on the (**a**) sulfur content and (**b**) desulfurization rate of high-sulfur bauxite.

As shown in Figure 9a, with an increase in the calcination temperature, the negative divalent sulfur and total sulfur content in high-sulfur bauxite decreased significantly, but the sulfur content in sulfate increased gradually. This is because increasing the temperature

in the same calcination time promotes the decomposition of pyrite [28]. Sulfate exhibits good thermal stability and cannot be decomposed at <650 °C. Upon the decomposition of diaspore, siderite, pyrite, and other substances in high-sulfur bauxite, the relative content of sulfate increased, in turn increasing the relative content of sulfur in sulfate. As shown in Table 4, at a calcination temperature of >550 °C, the negative divalent sulfur content in high-sulfur bauxite was <0.27 wt.%, which meets the requirements of the Bayer extraction process (<0.4 wt.%). At a calcination temperature of >600 °C, the negative divalent sulfur in high-sulfur bauxite was almost completely removed. Figure 9b shows that the predicted desulfurization rate of high-sulfur bauxite using the kinetic equation (Equation (4)) is consistent with the experimental data, with a maximum deviation of −3.26%, indicating that the kinetic model is reasonable.

3.3.2. XRD Analysis

The XRD patterns of the roasted high-sulfur bauxite ore are shown in Figure 10.

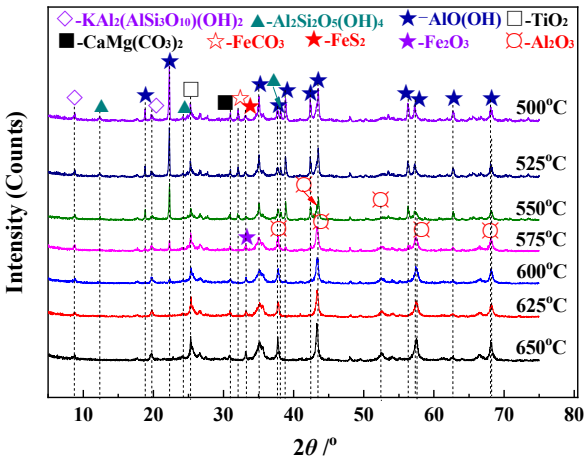


Figure 10. XRD patterns of roasted high-sulfur bauxite at different temperatures.

As shown in Figure 10, diaspore, kaolinite, siderite, and pyrite were all decomposed by transport-bed calcination in the range of 500 °C–650 °C, while muscovite, rutile, and dolomite showed no obvious changes. The decomposition of kaolinite was completed at 550 °C with an increase in the calcination temperature for a calcination time of 3.5 s. Siderite and pyrite were largely converted to Fe_2O_3 at 575 °C. The decomposition of diaspore continued up to around 600 °C, but obvious Al_2O_3 diffraction peaks began to appear at 550 °C. The results indicate that the XRD data are basically consistent with the data shown in Figure 5.

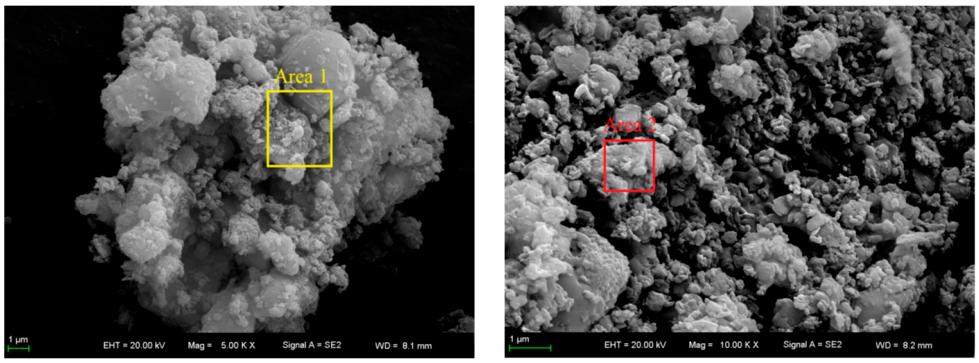
3.3.3. SEM Analysis

Figure 11 shows SEM images of the high-sulfur bauxite raw ore before and after roasting at 650 °C. The EDS analysis of area 1 and area 2 are shown in Figure 12.

The elemental analysis results of area 1 and area 2 by EDS are shown in Table 5.

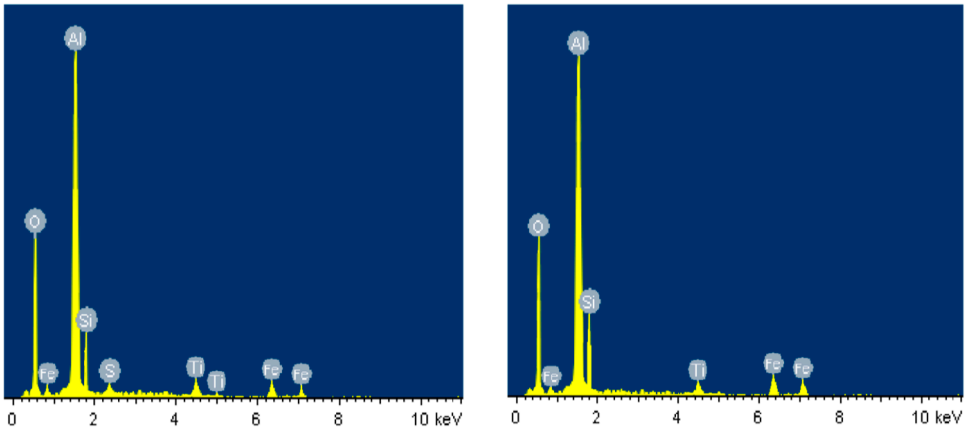
Table 5. Elemental analysis results of area 1 and area 2.

Area	O (wt.%)	Al (wt.%)	Si (wt.%)	Ti (wt.%)	Fe (wt.%)	S (wt.%)
Area 1	39.79	42.13	10.24	1.24	1.35	1.37
Area 2	37.54	43.81	12.06	1.15	1.67	-



(**a**) (**b**)

Figure 11. SEM images of high-sulfur bauxite (**a**) before and (**b**) after calcination.



(**a**) (**b**)

Figure 12. EDS analysis of (**a**) area 1 and (**b**) area 2.

The raw ore particles of high-sulfur bauxite have a dense structure and a few pores with diameters of 1–3 µm. After calcination of the ore in the conveyor bed, the large particles were significantly reduced in size to small fine particles, and the pore size was significantly increased. High-sulfur bauxite underwent dehydroxylation, decarburization, desulfurization, and other reactions, forming more micropores and increasing the specific surface area of the material during the calcination process, which was beneficial to the dissolution of alumina.

3.3.4. Alumina Digestion Analysis

The alumina digestion performance of high-sulfur bauxite after desulfurization is an important indicator to determine whether it can be applied in the Bayer process. The digestion effect of alumina was characterized by the relative dissolution rate. The analysis results of the relative dissolution rate of alumina in roasted high-sulfur bauxite ore are shown in Figure 13.

As shown in Figure 13, the relative dissolution rate of alumina in high-sulfur bauxite increased significantly with an increase in the calcination temperature. At a calcination temperature of >600 °C, the relative dissolution rate was $\leq$99%. This phenomenon is directly related to the degree of decomposition of diaspore. The decomposition of diaspore led to the destruction of the original crystal lattice, resulting in the formation of alumina with high activity but poor crystallinity [3]. For the same calcination time, the higher the calcination temperature, the higher the decomposition rate, leading to an increase in the relative dissolution rate of alumina.

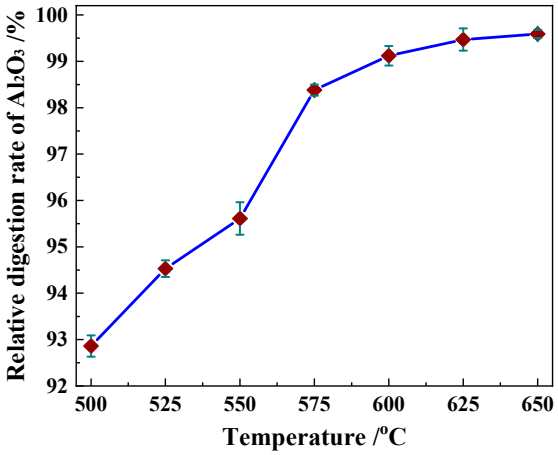


Figure 13. Relative dissolution rate of alumina in roasted high-sulfur bauxite.

4. Conclusions

(1) At calcination temperatures <650 °C, the main reactions were the dehydroxylation of diaspore and kaolinite, in addition to the decomposition of siderite and pyrite. These reaction temperatures overlapped and could not be separated.

(2) The desulfurization reaction followed a three-dimensional spherical diffusion mechanism, with the reaction rate controlled by the rate of diffusion of O_2 or SO_2 through the solid product layer.

(3) The negative divalent sulfur content in high-sulfur bauxite was <0.03 wt.% after using a conveyor-bed calcination system in the range of 600 °C–650 °C for around 3.5 s. The desulfurization rate was >0.98, and the relative dissolution rate was >99%. The prediction of the desulfurization rate by the kinetic model was in agreement with the experimental data.

Author Contributions: Conceptualization, Y.C. and S.J.; methodology, S.J.; validation, S.J., Y.C. and B.Z.; investigation, S.J. and B.Z.; data curation and writing, S.J.; visualization, S.J. All authors have read and agreed to the published version of the manuscript.

Funding: This research was funded by Shaanxi Provincial Innovation Capability Support Program (Grant No. 2021TD-53) in China.

Institutional Review Board Statement: Not applicable.

Informed Consent Statement: Not applicable.

Data Availability Statement: Data are available on request from the authors.

Acknowledgments: The authors would like to thank Chang Chen for his help in the submission process of this paper.

Conflicts of Interest: The authors declare no conflict of interest.

References

1. Hu, X.; Chen, W.; Xie, Q. Sulfur phase and sulfur removal in high sulfur-containing bauxite. *Trans. Nonferrous Met. Soc. China* **2011**, *21*, 1641–1647. [CrossRef]
2. Li, X.; Niu, F.; Liu, G.; Qi, T.; Zhou, Q.; Peng, Z. Effects of iron-containing phases on transformation of sulfur-bearing ions in sodium aluminate solution. *Trans. Nonferrous Met. Soc. China* **2017**, *27*, 908–916. [CrossRef]
3. Zhao, B.; Chen, Y.; Jiu, S. Effective Desulfurization and Alumina Digestion of High-Sulfur Bauxite by New Roasting Process with Conveying Bed. *Processes* **2021**, *9*, 390. [CrossRef]
4. Liu, Z.; Yan, H.; Ma, W.; Xiong, P. Sulfur Removal of High-Sulfur Bauxite. *Min. Met. Explor.* **2020**, *37*, 1617–1626. [CrossRef]
5. Zhou, X.; Tan, F.; Chen, Y.; Yin, J.; Xia, W.; Huang, Q.; Gao, X. Thermodynamic analysis of Na−S−Fe−H_2O system for Bayer process. *Trans. Nonferrous Met. Soc. China* **2022**, *32*, 2046–2060. [CrossRef]
6. Yuan, J.; Chen, C.; Li, J.; Quan, B.; Lan, Y.; Wang, L.; Fu, H.; Gai, J. Initial Corrosion Behavior of 12Cr1MoV Steel in Thiosulfate-Containing Sodium Aluminate Solution. *Metals* **2020**, *10*, 1283. [CrossRef]

7. Xie, Q.; Chen, W.; Yang, Q. Corrosion behavior of four kinds of steels in sulfide-containing Bayer liquor. *J. Cent. South Univ. Sci. Technol.* **2014**, *45*, 2560–2565.
8. Zhang, N.; Jiang, H.; Wu, X. Research on disposing of sulfur of high grade bauxite containing sulfur in Guizhou. *Light Met.* **2007**, *7*, 7–10.
9. Bulut, G.; Arslan, F.; Atak, S. Flotation behaviors of pyrites with different chemical compositions. *Min. Met. Explor.* **2004**, *21*, 86–92. [CrossRef]
10. Wang, C.; Zhang, Q.; Mao, S.; Qin, S. Effects of Fine Minerals on Pulp Rheology and the Flotation of Diaspore and Pyrite Mixed Ores. *Minerals* **2020**, *10*, 60. [CrossRef]
11. Chai, W.; Huang, Y.; Peng, W.; Han, G.; Cao, Y.; Liu, J. Enhanced separation of pyrite from high-sulfur bauxite using 2-mercaptobenzimidazole as chelate collector: Flotation optimization and interaction mechanisms. *Miner. Eng.* **2018**, *129*, 93–101. [CrossRef]
12. Qing, S.; Shuai, W.; Xin, M.; Hong, Z. Desulfurization in high-sulfur bauxite with a novel thioether-containing hydroxamic acid: Flotation behavior and separation mechanism. *Sep. Purif. Technol.* **2021**, *275*, 119147.
13. Liu, Z.; Li, D.; Ma, W.; Yan, H.; Xie, K.; Zheng, L.; Li, P. Sulfur removal by adding aluminum in the bayer process of high-sulfur bauxite. *Miner. Eng.* **2018**, *119*, 76–81. [CrossRef]
14. Hu, X.; Chen, W.; Xie, Q. Desulfuration of high sulfur bauxite by oxidation roasting. *J. Cent. South Univ. Sci. Technol.* **2010**, *3*, 852–858.
15. Lu, D.; Lyu, G.; Zhang, T.; Zhang, W.; Xie, D.; Wang, Y.; Wang, L. Roasting Pretreatment-Low Temperature Digestion Method for Comprehensive Utilization of High-Sulfur Bauxite. In *Light Metals 2018*; Springer International Publishing: Cham, Switzerland, 2018; pp. 3–6.
16. Lv, G.; Zhang, T.; Bao, L.; Dou, Z.; Zhao, A.; Qu, H.; Ni, P. Roasting pretreatment of high-sulfur bauxite and digestion performance of roasted ore. *Chin. J. Nonferrous Met.* **2009**, *19*, 1684–1689.
17. Lou, Z.; Xiong, Y.; Feng, X.; Shan, W.; Zhai, Y. Study on the roasting and leaching behavior of high-sulfur bauxite using ammonium bisulfate. *Hydrometallurgy* **2016**, *165*, 306–311. [CrossRef]
18. Jin, H.; Wu, F.; Li, J.; Chen, C.; Liu, H.; Yang, Q. Desulfurization of pyrite in high-sulfur bauxite with microwave roasting process. *J. Cent. South Univ. Sci. Technol.* **2020**, *51*, 2707–2717.
19. Budrugeac, P. On the use of the model-free way method for kinetic analysis of thermoanalytical data–advantages and limitations. *Thermochim. Acta* **2021**, *706*, 179063. [CrossRef]
20. John, P.; Patrick, K. Kinetic analyses using simultaneous TG/DSC measurements: Part I: Decomposition of calcium carbonate in argon. *Thermochim. Acta* **2002**, *388*, 115–128.
21. Zhao, Y.; Zhang, J.; Sun, T.; Shan, Y.; Zhao, H. Reduced equations to estimate kinetic parameters from non-isothermal TG-DTG or DSC curves. *Thermochim. Acta* **1993**, *223*, 101–108.
22. Cheng, H.; Liu, Q.; Huang, M.; Zhang, S.; Frost, R.L. Application of TG-FTIR to study SO_2 evolved during the thermal decomposition of coal-derived pyrite. *Thermochim. Acta* **2013**, *555*, 1–6. [CrossRef]
23. Cheng, S.; Jiu, S.; Li, H. Kinetics of Dehydroxylation and Decarburization of Coal Series Kaolinite during Calcination: A Novel Kinetic Method Based on Gaseous Products. *Materials* **2021**, *14*, 1493. [CrossRef] [PubMed]
24. Vyazovkin, S.; Wight, C. Isothermal and nonisothermal kinetics of thermally stimulated reactions of solids. *Int. Rev. Phys. Chem.* **1998**, *3*, 407–433. [CrossRef]
25. Hu, R.; Shi, Q. *Thermal Analysis Kinetics*, 1st ed.; Science Press: Beijing, China, 2001; pp. 127–131.
26. Blaine, R.; Kissinger, H. Homer Kissinger and the Kissinger equation. *Thermochim. Acta* **2012**, *540*, 1–6. [CrossRef]
27. Juan, J.; Francisco, P.; Guillermo, R. On the integration of kinetic models using a high-order Taylor series method. *J. Chemom.* **1992**, *6*, 231–246.
28. Zhang, X.; Kou, J. A comparative study of the thermal decomposition of pyrite under microwave and conventional heating with different temperatures. *J. Anal. Appl. Pyrolysis* **2019**, *138*, 41–53. [CrossRef]